NANO LETTERS

2008
Vol. 8, No. 4
1047-1054

Protonation Effects on the Branching Ratio in Photoexcited Single-Walled Carbon Nanotube Dispersions

Jeffrey L. Blackburn,* Timothy J. McDonald, Wyatt K. Metzger, Chaiwat Engtrakul, Garry Rumbles, and Michael J. Heben

National Renewable Energy Laboratory, Golden, Colorado 80401

Received October 30, 2007; Revised Manuscript Received January 11, 2008

ABSTRACT

The ensemble PL quantum yield for raw single-walled carbon nanotubes (SWNTs) dispersed in sodium cholate (SC) is ~5 times greater than that for the same raw SWNTs dispersed in sodium dodecyl sulfate (SDS) and ~10 times greater than the quantum yield of purified SWNTs dispersed in SC. Absorbance and Raman spectra indicate that purified SC-dispersed SWNTs and raw SDS-dispersed SWNTs are hole-doped by protonation. Experiments comparing PL emission efficiency using E_2 and E_1 excitation show that protonation significantly affects the $E_2 \rightarrow E_1$ relaxation process, which has typically been assumed to occur with unit efficiency. The $E_2 \rightarrow E_1$ relaxation is 5 times more efficient in producing E_1 PL when SWNTs are unprotonated and protected by the SC surfactant. The results provide clear evidence that extrinsic factors, such as residual acids and the specific nature of SWNT-surfactant and SWNT-solvent interactions, can significantly affect measured SWNT luminescence quantum yields.

Single-walled carbon nanotubes (SWNTs) are being considered for use in photovoltaics,[1,2] light-emitting diodes,[3] field effect transistors,[4] and as bioimaging agents.[5] With these applications in mind, the fundamental processes of absorption and luminescence are being extensively studied. Of particular importance for solar energy conversion is the question of how, and the rate at which, the energy contained in photoexcited states is dissipated. If recombination pathways are fast compared to the rate at which excitons can be separated and charge carriers harvested, then it will be difficult to use the energy contained in photoexcited states to do electrical or chemical work.

Without forming junctions and making contacts, which may be required for exciton dissociation and carrier harvesting, the photoluminescence (PL) quantum yield (φ_{PL}) can comment on the competition between radiative and nonradiative relaxation pathways. Early studies reported φ_{PL} for SWNTs dispersed in aqueous solutions to be $\sim 10^{-4}$ to 10^{-3} (0.01–0.1%).[6–9] Subsequent studies demonstrated that extrinsic factors such as SWNT length,[10] sidewall defects, and/or protonation,[11] residual bundles,[12] and the large nonresonant background present in the absorbance spectra of bulk dispersions[13] may contribute to the low values initially reported. More recent efforts aimed at overcoming these external influences have reported higher values of ~1−1.5% for SWNT dispersions,[12,13] 3–7% for single tubes isolated on substrates,[14,15] and up to 10% for particularly bright, individual SWNTs in solution.[11]

The mechanisms responsible for the observed variations in PL quantum yield are not well-known. To date, φ_{PL} measurements have been performed by quantifying the emission from the first excitonic state (E_1) after photoexcitation of the second excitonic transition (E_2). Thus, many kinetic factors could affect the measured PL quantum yield, including any competitive pathways by which E_2 or E_1 excitons may be quenched. An important issue that has not been experimentally addressed is the efficiency with which E_2 excitons relax to the E_1 state. In the absence of direct experimental observation, the relaxation is typically assumed to occur with 100% efficiency.[11]

Here, we demonstrate that protonation dramatically reduces (by at least a factor of 5) the $E_2 \rightarrow E_1$ relaxation efficiency in surfactant-stabilized dispersions of SWNTs. This conclusion was made possible by first determining that as-received *purified* HiPCO SWNTs exhibit dramatically lower φ_{PL} as compared to raw HiPCO SWNTs when dispersed as noninteracting individuals in sodium cholate. A detailed Raman spectroscopy analysis demonstrated that the results could not be ascribed to bundling phenomena and that, instead, differences in the degree of residual sidewall protonation were responsible. Then, by measuring the E_1 emission intensity following either E_2 or E_1 excitation, we determined that the efficiency of relaxation from the E_2 state to the luminescent E_1 state is dramatically lower for the purified,

* Corresponding author. E-mail: jeffrey_blackburn@nrel.gov.

10.1021/nl072809g CCC: $40.75
Published on Web 03/05/2008

protonated SWNTs as compared to raw, unprotonated SWNTs. Unintentional sidewall protonation also occurs in some loosely bound surfactant systems, such as SDS, and dramatically lowers the PL quantum yield. In agreement with the most recent literature, we found that the ensemble quantum yield with E_2 excitation reaches a maximum of ~1–1.5% for several tubes within the raw SC dispersion when protonation is minimized. Together, these results provide much-needed insight into the wide range of φ_{PL} values reported for SWNTs in the literature.

As-produced ("raw") and purified HiPCO SWNTs were purchased from Carbon Nanotechnologies Incorporated (CNI). Although the exact methods used by CNI are proprietary, it is known that the purified SWNTs have been treated with acid(s) to remove residual metal catalyst particles. SWNT dispersions in D_2O were produced by ultrasonication of ~20 mg of SWNT material in 1 wt % solutions of sodium cholate (SC) or sodium dodecyl sulfate (SDS). A Cole Palmer 750 W sonicator was used, with a $^1/_4$ in. ultrasonic tip operating at 40% power. The solutions were sonicated for 40 min while the sample was cooled by 20 °C water flowing in an external jacket. An aggressive centrifugation at 28000 rpm (141000*g*), using a swing bucket (SW28) rotor in a Beckman centrifuge for 4 h, was employed in an effort to remove all bundled tubes from solution.[6] Stable SWNT dispersions were decanted and investigated in 1 cm cuvettes. Absorption spectra were obtained with a Shimadzu UV-3600 spectrometer. Raman spectra for the dispersions were recorded in backscattering configuration, with excitation at 532 nm by a frequency-doubled YAG laser.[16] Photoluminescence spectra were obtained in front-face configuration using a modified Fourier transform instrument with excitation provided by a tungsten lamp coupled to a monochromator[17] or a Nd:YVO laser operating at 1064 nm. Relative quantum yield responses were compared using solutions with the same optical densities, while absolute quantum yields were obtained by measuring the absorption and PL spectra of a reference dye IR no. 26,[18] which has a reported quantum yield of ~5×10^{-3} in dichloroethane.[19]

Figure 1a shows absorption spectra for raw SWNTs dispersed with SC (raw SC-SWNTs), purified SWNTs dispersed with SC (purified SC-SWNTs), and raw SWNTs dispersed with SDS (raw SDS-SWNTs). The interband transitions for the different semiconducting (E_1, E_2, and E_3) and metallic species (M_1) appear as peaks that vary in sharpness and intensity depending on the details of the local environments within the dispersions. Note that the optical densities of the samples were purposefully adjusted to be nearly the same in the E_2 region and, as a result, the spectra also overlay in the short wavelength region. Presentation of the data in this manner shows clearly that the E_1 transitions for the raw SC-SWNTs are substantially more intense relative to the E_2 transitions, while the E_1 transitions for the raw SDS-SWNT and purified SC-SWNTs dispersions are substantially reduced in intensity. The peaks from the raw SC-SWNTs are quite intense and well-resolved, demonstrating that the degree of SWNT isolation is excellent in this sample.

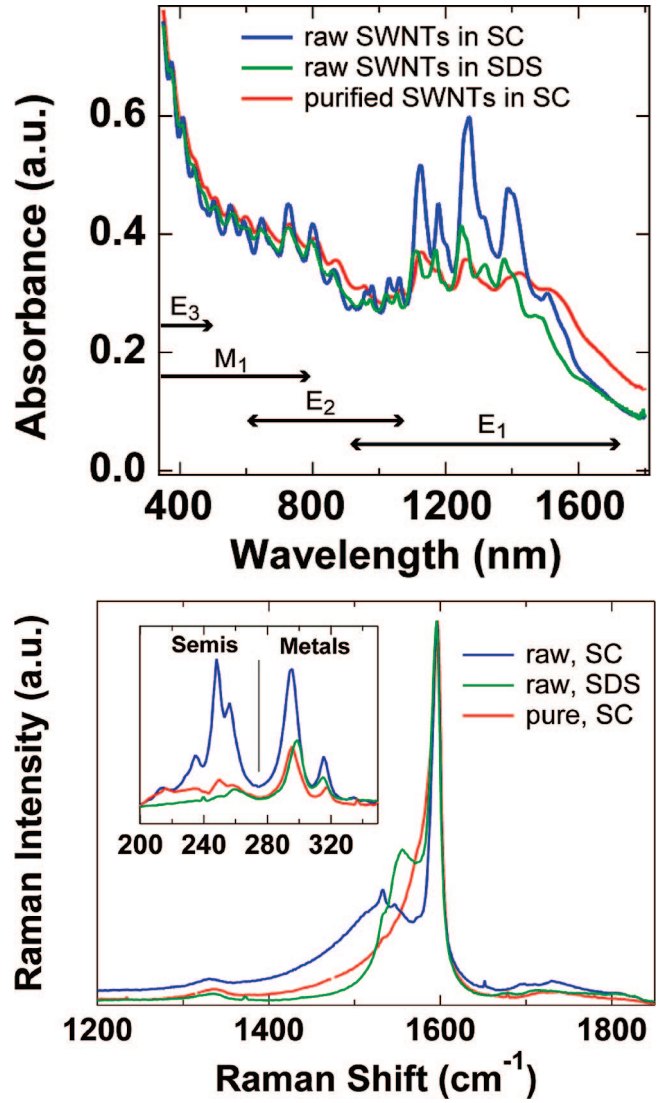

Figure 1. (a) Absorbance spectra of raw HiPCO SWNTs dispersed with sodium cholate (SC) or sodium dodecyl sulfate (SDS) and purified SWNTs dispersed with SC. Arrowed regions show the approximate regions for semiconducting (E_1, E_2, E_3) and metallic (M_1) transitions. (b) Raman spectra in the G-band region of the three dispersions excited at 532 nm. G-band spectra are normalized to the G^+ peak at 1592 cm^{-1}. Inset shows the un-normalized Raman spectra in the RBM region.

Before evaluating and comparing the PL efficiencies from the different samples (vide infra), we must consider two possible factors that could lead to the differences in the absorption spectra seen in Figure 1a, i.e., bundling and doping effects. Bundling must be considered first because PL from bundled tubes may be quenched by tube−tube interactions, which would lead to an underestimation of φ_{PL}. A straightforward comparison of φ_{PL} values becomes impossible if the concentration of bundled SWNTs is not nearly zero, or at least known and constant, in the three dispersions. Several pieces of data show that the SWNTs under study here are not appreciably bundled. First, note that the E_2 peaks in all samples overlap nearly exactly and that the E_1 transitions of the pure SC-SWNTs and raw SDS-SWNTs are reduced in intensity but not significantly red-shifted relative to the raw SC-SWNTs. Significant red-shifting of

both E_1 and E_2 transitions is expected when tubes are bundled.[6] To test this assertion explicitly, we dialyzed a sample of raw SDS-SWNTs against pure water to remove SDS and induce bundling and observed the expected red-shift in the E_1 transitions (see Supporting Information, Figure S1a). In contrast, in the absence of changing surfactant concentrations, the raw SDS-SWNTs dispersion is quite stable, showing a virtually unchanged absorbance spectrum after three years (Supporting Information, Figure S1b). Another expectation for bundling is significant energy transfer from smaller diameter tubes to large ones.[6] In this case, one expects the PL emission spectrum to differ in shape from the absorption spectrum, with substantially more emission on the low energy side, but this is not observed for any of the samples (Supporting Information, Figure S2a−c). All of these results are consistent with cryo-TEM images of centrifuged SDS-SWNTs, which show no bundling.[20] Consequently, we can conclude with confidence that the SWNTs observed here via absorption, Raman, and PL spectroscopies are unbundled individuals.

With bundling effects excluded, we can now consider how the electronic properties of the micelle-encapsulated SWNTs may vary among the three dispersions. Diminished E_1 intensities are well-documented effects for SWNT dispersions exposed to acids.[21,22] The reduction in optical density (bleaching) in the E_1 transitions results from a lowering of the Fermi level due to hole-doping associated with protonation.[22] Note that the type of interaction under consideration here is not associated with the formation of any new C−H covalent bonds. Ramesh et al. studied the interaction of SWNTs with acids and described protonation as a completely reversible charge-transfer process in which C:H+ moieties formed and caused the localization of electronic charge in response to the proton.[23] As a result, the SWNTs become hole-doped. This type of protonation is an electronic effect that is completely reversible and does not result in a permanent change in nanotube structure or the permanent removal of electrons. In this context, the reduced E_1 intensities for the pure SC-SWNTs can be ascribed to hole-doping due to residual protonation associated with the purification process.[24]

To probe this issue further, we performed solution-phase Raman spectroscopy and analyzed the G-band region of the spectra for the three different dispersions (Figure 1b, mainframe). Focusing first on the data for the raw SC-SWNTs, a sharp G^+ mode at 1592 cm^{-1} and a broad G^- mode near 1530 cm^{-1} are seen, corresponding to semiconducting and metallic SWNTs, respectively. The broad G^- peak is asymmetric, returns slowly to baseline on the low energy side, and is fit well by a Breit–Wigner–Fano (BWF) line shape. Recently, we showed that a broadened, red-shifted G^- peak can be present for surfactant isolated laser SWNTs and that its line shape is dependent on the surfactant used and the degree to which electron density is polarized at the SWNT surface.[16] Since then, single-tube studies have elegantly shown that the energy and width of the G^- mode critically depend on the Fermi energy of the metallic SWNTs, which, similar to the situation for graphene,[25] determines the energy window for coupling of the G phonon to electronic excitations near the Dirac point.[26,27] The energy and width have a minimum and maximum, respectively, when the Fermi energy is at the Dirac point and, under such conditions, the SWNT may be considered to be intrinsic (undoped). As the Fermi energy is moved away from the Dirac point to either higher or lower energy (n- or p-type doping, respectively), the G^- mode narrows and blue-shifts, providing a useful qualitative indicator of intentional or unintentional doping. Interestingly, the G^- mode from the raw SC-SWNTs is broad (fwhm $\sim$ 80 cm^{-1}) and located at $\sim$1530 cm^{-1}, which is not blue-shifted in comparison to the expected value for the HiPCO diameter range.[28,29] Thus, we can conclude that the Fermi energy is close to the Dirac point for the metallic SWNTs, which suggests that the Fermi energy for the semiconducting SC-SWNTs is also near the middle of the gap. Consequently, the G-band Raman data indicates that the raw SC-SWNTs are nearly intrinsic and not significantly doped.

In contrast, the BWF line shape is virtually absent for the purified SC-SWNTs (Figure 1b). In this case, the G-band spectrum is dominated by the semiconducting G^+ mode, with a small shoulder for the G^- band that can be fit fairly well by a Lorentzian line shape or a low-intensity blue-shifted BWF line shape with a small coupling parameter ($-1/q$). Interestingly, the differences in the G^- spectra between the raw and purified SC-SWNTs are the same as those observed for raw and purified HiPCO SWNTs in their dry form, before dispersion, as shown in the Supporting Information (Figure S3). Similar findings have been reported in other studies of hole-doping by acids.[21,22,30] Once again, this effect is described by a lowering of the Fermi energy, which narrows the energy window over which the G^- phonon may couple to electronic excitations near the Dirac point. These results establish that the purified HiPCO SWNTs are significantly hole-doped as purchased. Evidently, the purified SWNTs remain hole-doped even after intense sonication and dispersion by surfactants in aqueous solutions, implying the protons introduced by purification remain associated with the SWNT surfaces, in agreement with our previous study.[24]

The evidence for protonation in purified SC-SWNT dispersions is also supported by analysis of the Raman radial breathing modes (RBMs) (Figure 1b, inset). The 532 nm wavelength used here probes the RBMs of both metallic and semiconducting species in the HiPCO dispersions ($\sim$0.8–1.2 nm). The RBM peaks in the 220–270 cm^{-1} range correspond to semiconducting tubes excited resonantly via the third excitonic transition (E_3), while peaks from $\sim$280–320 cm^{-1} correspond to metallic tubes excited via the first metallic resonance (M_1). The data shows a significantly attenuated response for the purified SC-SWNTs (relative to the raw SC-SWNTs) in both the semiconducting and metallic tubes. This effect is commonly seen in acid-treated samples where lowering of the Fermi level modifies the resonance enhancement for tubes to varying degrees, leading to diameter-dependent attenuation of the RBM intensity.[21] RBM attenuation is most severe, and nearly complete, for the smaller band gap (larger diameter) semiconducting tubes because the

Fermi level is lowered well into the valence band. Thus, the responses of both the BWF and RBM modes support the conclusion that the purified SC-SWNTs are hole-doped by the retained acid.

Interestingly, despite the fact that the raw SDS-SWNTs were not purposefully exposed to acids, their Raman spectroscopy is quite similar to that of the purified SC-SWNTs (Figure 1b). The metallic G^- mode for the raw SDS-SWNTs is narrow and symmetric and does not require a BWF line shape. The RBM modes are also strongly attenuated (Figure 1b, inset), suggesting that the resonance conditions are changed similarly for raw SDS-SWNTs and purified SC-SWNTs. A natural conclusion is that raw SWNTs become hole-doped during preparation when SDS is the surfactant. This unanticipated oxidation can be attributed to the lability of the SDS molecules, which may allow for water molecules and/or protons, even at near neutral pH, to access the SWNT surface and polarize electron density. Consistently, larger diameter, raw laser-oven SWNTs that bind SDS more weakly[31] show an even greater bleaching of the E_1 optical density (Supporting Information, Figure S4) and also show the hallmarks of hole-doping in Raman spectroscopy.[16] SC is known to produce darker SWNT solutions, and the stronger binding and more complete surfactant sheath provided by SC molecules evidently protects the raw SC-SWNTs from becoming hole-doped (Figure 1b). Interestingly, water itself may be able to produce quenching of the E_1 transitions by hole-doping. Recent cross-polarization NMR experiments on ^{13}C-doped laser-oven SWNTs show that water molecules are surprisingly proximal to laser SWNTs even in strongly base-neutralized Nafion films, which suggests a weak dipolar interaction and electronic polarization even in the absence of free protons.[32]

With the understanding that the differences observed in Figure 1 are due to electronic effects associated with protonation rather than bundling effects, we can consider the PL responses of the three types of dispersions. Figure 2 shows the two-dimensional PLE maps where bright spots show emission from the first excitonic transition (E_1) of each specific SWNT species after resonant excitation at the second excitonic transition (E_2). Approximately 30 different species are observed and assigned according to Weisman et al.[33] As noted previously, the optical density of each sample was deliberately adjusted to be approximately equal in the E_2 excitation region (Figure 1a). Thus, in the absence of bundling, the maps offer a direct comparison of the relative PL quantum yields. Specifically, it is immediately obvious that φ_{PL} of the brightest species in the raw SC-SWNT sample is ~5 times greater than that of the same species in the raw SDS-SWNT sample and ~10 times greater than φ_{PL} of the purified SWNTs in SC.

Although Figure 2 demonstrates a dramatic effect of protonation on the relative PL quantum yields, the *mechanism* by which protonation reduces the PL quantum yield is not immediately obvious. Following Ma et al.,[34] Figure 3 displays a scheme of various processes that may occur in a typical PL experiment when SWNTs are excited via the E_2 transition. Accordingly, the quantum yield of SWNT luminescence can be expressed as:

$$\varphi_{PL} = \frac{k_r}{\sum_{i=0}^{j} k_i} = \frac{k_r}{k_r + k_{nr} + k_q[Q]} \quad (1)$$

In eq 1, k_r is the rate of radiative recombination and k_i represents each of the total j rates by which the first excitonic state may be depopulated. In addition to the radiative transition, the k_i term includes nonradiative pathways such as intersystem crossing, nonradiative annihilation, trapping, etc., all of which can combine additively to give the k_{nr} rate, and also a quenching term equal to the product of the quenching rate, k_q, and concentration of quenching species, [Q]. Thus, any change in the relative rates of these E_1 depopulation pathways will affect the measured quantum yield. While eq 1 accounts for depopulation of the first excitonic state, we must also consider the efficiency with which the first state is populated from relaxation of the second excitonic state. The population density of excitons reaching E_1 is determined by the branching ratio for depopulation of the E_2 state. Similar to eq 1, this branching ratio may be expressed as the rate of $E_2 \rightarrow E_1$ relaxation (k_{21}) relative to all rates associated with other processes that may depopulate E_2, which combine to give the rate k_{2x} in Figure 3. If environmental factors cause excitons to be diverted from E_2 to states other than E_1 (e.g., E_x in Figure 3), the quantum yield for $E_2 \rightarrow E_1$ relaxation is less than unity and the measured luminescence quantum yield will be lowered. Possible nonemissive states include dark states forbidden by single photon excitation, trap states, or an electron–hole continuum.[34–36]

With the scheme of Figure 3 in mind, we employed several experiments to explore the mechanism controlling the large variations in the PL quantum yield among the SWNT dispersions. We first performed time-resolved luminescence as described previously[7,37] on several SWNT species in both the raw and purified SC-SWNTs dispersions. Surprisingly, the PL lifetimes were not significantly different in the two different types of samples. For example, the PL decay from the (7,5) SWNT was fit by dominant lifetimes of 113 and 108 ps for the raw and purified samples, respectively. These values are close to the 140 ps previously reported for the SDS-dispersed (7,5) tube.[7] Such minor changes in the measured PL lifetime suggest that, at least for the "bright" SWNTs measured in the TRPL experiment, the environment does not significantly affect the relative rates for depopulation of the E_1 state. These small lifetime changes cannot account for the dramatic differences in the PL quantum yield.

We next explored the role of the $E_2 \rightarrow E_1$ branching ratio by comparing the quantum yield for emission with excitation at E_1 to the quantum yield with excitation at E_2. Measurement of E_1 PL with direct excitation into the E_1 level has not been reported previously due to the experimental difficulties associated with selectively exciting the E_1 and rejecting the excitation light from the PL detector. To overcome this difficulty, we used a Nd:YVO_4 laser (1064 nm), which is resonant with the E_1 transition of the (10,2) tube. Fortu-

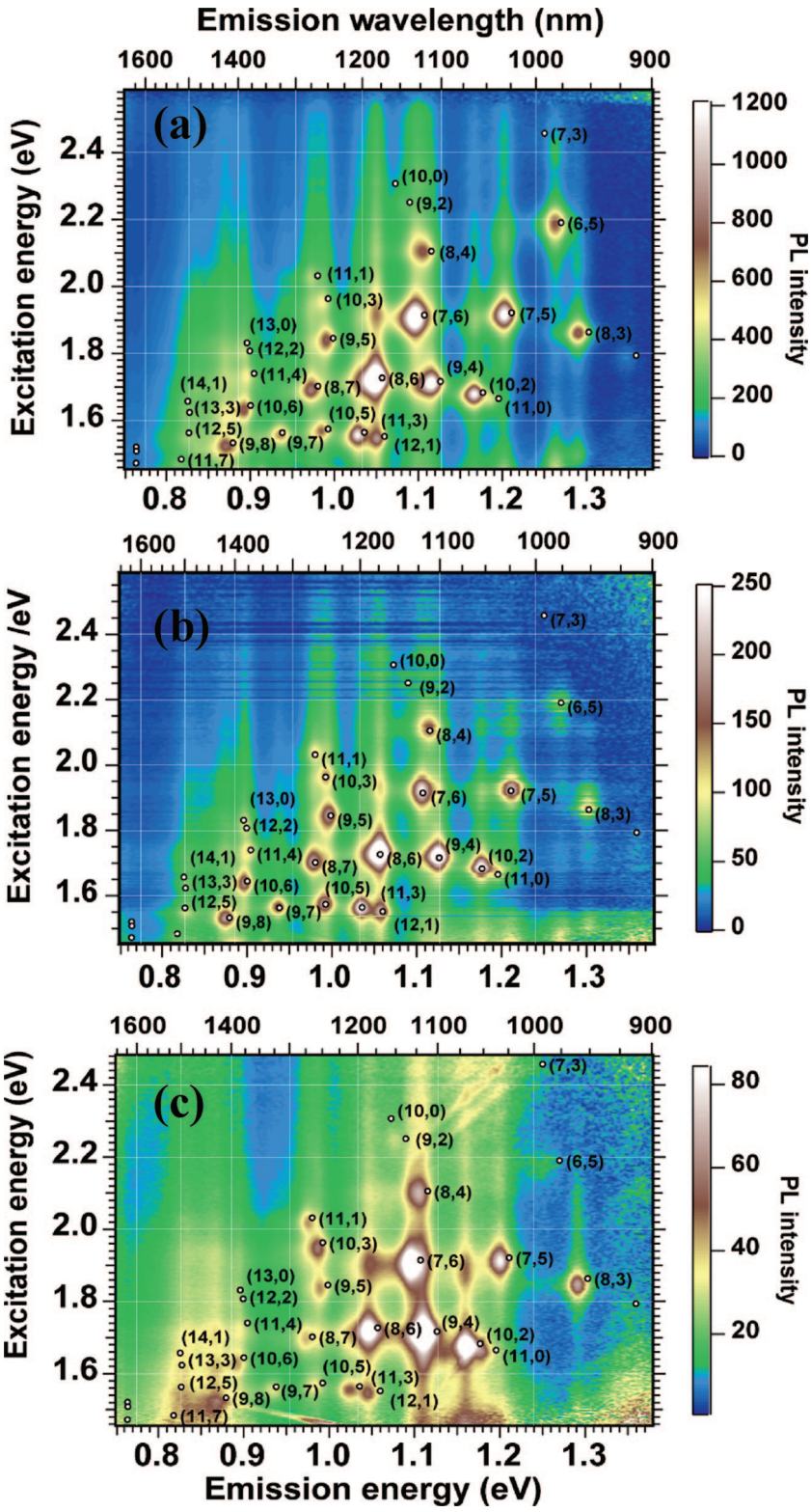

Figure 2. Photoluminescence excitation (PLE) spectra of (a) raw SC-dispersed HiPCO SWNTs, (b) raw SDS-dispersed HiPCO SWNTs, and (c) purified SC-dispersed HiPCO SWNTs. Note the different intensity scales shown on right.

itously, no other tubes in the distribution possess E_1 transitions within ±40 nm of the 1064 nm excitation. The excitation light was rejected using a 1064 nm holographic notch filter placed between the sample and the detector. With this arrangement, we were able to measure the relative PL quantum yields for the (10,2) SWNT after E_1 excitation of both raw and purified SC-SWNT (Figure 4a). Once again, the sample concentrations were adjusted to make the optical densities in the absorption spectra equal at 1064 nm. Because PL from the E_1 transition of the (10,2) tube was seen on either side of the notch filter's ~25 nm window, we used a Voigt line shape to fit the wings of the PL from each sample

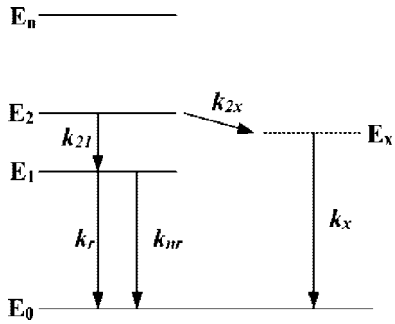

Figure 3. Schematic description of the possible excitonic processes following photoexcitation of a surfactant-encapsulated SWNT, from Ma et al.[34] In a typical PLE experiment, the SWNT absorbs a photon that populates the E_2 exciton state. This exciton may decay to the lowest energy E_1 exciton state with rate k_{21} or may decay with rate k_{2x} to a nonluminescent state E_x, which then decays nonradiatively with rate k_x. E_1 excitons may recombine radiatively with rate k_r or nonradiatively with rate k_n, or may be quenched by other species, Q, in solution, with rate k_q[Q] (not shown).

(dashed line, Figure 4). Note that the Voigt profile parameters needed to fit the E_1 emission profile were nearly identical to those required to fit the emission found with E_2 excitation. Surprisingly, the integrated PL intensity following E_1 excitation was only 1.8 times higher for the raw SC-SWNTs as compared to the purified SC-SWNTS. This ratio is dramatically lower than the ~10:1 ratio observed for E_2 excitation, as shown in Figure 4b. This result suggests that the efficiency of the $E_2 \rightarrow E_1$ relaxation is dramatically reduced by the electronic effects associated with protonation.

To further probe the effect of protonation on the $E_2 \rightarrow E_1$ branching ratio, we performed an experiment in which the SWNTs were slowly deprotonated by reaction with added hydrogen peroxide.[24] The slow kinetics of the deprotonation reaction can be followed as a slow rise in the PL intensity when the purified SC-SWNT sample is excited via the E_2 transition, as shown for three SWNT species in Figure 4c. Here we plot the PL intensity normalized to 1-transmission (1-T) to account for the fact that some SWNTs aggregate and fall out of solution during this ~10 h exposure to peroxide. We repeated this experiment for E_1 excitation of the purified (10,2) SC-SWNT at 1064 nm. Remarkably, in this case, the E_1-excited PL intensity remained nearly constant during the same time period in which the E_2-excited PL intensity rose by ~25%. The observations suggest that the efficiency of the $E_2 \rightarrow E_1$ relaxation channel increases as protons are scrubbed away, while the efficiency of recombination across the gap is relatively unaltered. These results support the hypothesis that a dominant mechanism by which protonation reduces the PL quantum yield is by changing the branching ratio for excited-state relaxation, essentially lowering the number of excitons that reach the luminescent E_1 state following excitation into higher energy states.

It is interesting to consider how sidewall protonation could affect how E_2 excitons decay via pathways other than direct population of the E_1 state. It is clear that the vast majority of excitons do not reach the luminescent E_1 state following E_2 excitation of protonated SWNTs. The nonluminescent

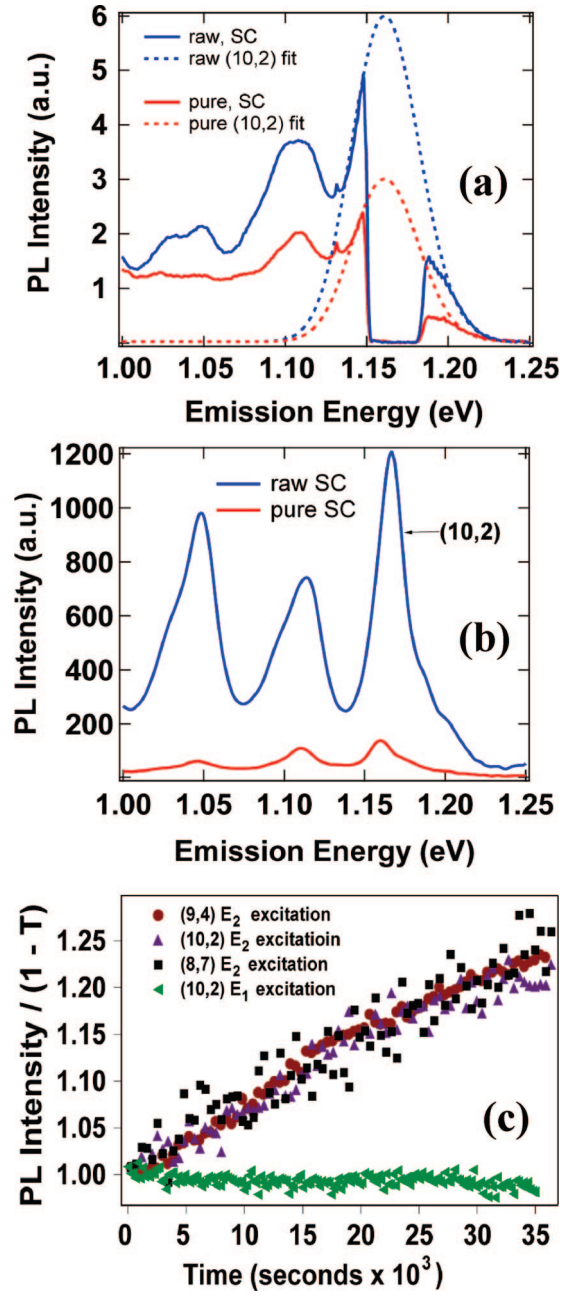

Figure 4. (a) E_1-excited PL spectra of raw and purified SC-SWNTs, excited with a 1064 nm (1.17 eV) Nd:YVO laser. Excitation light is blocked with a notch filter. Dashed lines show fits to PL of the (10,2) SWNT. (b) E_2-excited PL spectra of same samples. Excitation is at 743 nm (1.67 eV) (c) PL intensity for three SWNT species as a function of time for purified SC-SWNTs treated at $t = 0$ with hydrogen peroxide. The PL intensity is normalized to the absorptance (1-transmission) of each species to account for the time-dependent reduction in optical density (and PL) due to some SWNTs flocculating out of solution. The top three traces show SWNT PL following E_2 excitation, while the lowest trace shows the (10,2) PL following E_1 excitation.

states to which these excitons are shuttled are unclear, but possibilities include trap states and dark excitonic states between the E_2 and E_1. It is also possible that three-body Auger annihilation[38] may quench E_2 excitons more effectively than E_1 excitons. Predominant in quantum-confined systems, Auger recombination involves rapid energy transfer

Table 1. PL Quantum Yields, Calculated by Reference to IR26, of Several SWNT Species in the Raw SC-SWNT Dispersion

(*n*,*m*) assignment	quantum yield (%)	standard deviation	comment
(7,5)	1.3	0.24	
(7,6)	1.4	0.25	
(6,5)	0.92	0.08	
(8,6)	1.0	0.21	
(9,4)	0.95	0.20	
(8,3)	>0.5		no IR26 PL

from a photoexcited exciton to another exciton or charge carrier, which quenches PL from the photoexcited exciton. In a recent report, the Auger mechanism was suggested to account for PL quenching induced by SWNT protonation.[11] The efficiency of the Auger process should scale with the density of states available to the third body, in this case the hole created by protonation, scattered by the photoexcited exciton. Because the density of accepting states in the valence band increases with increasing energy from the band edge, E_2 Auger annihilation should rationally be more efficient than E_1 Auger annihilation.

Alternatively, we can speculate that E_2 excitons may be dissociated, producing free electrons and holes. The reduced Coulombic coupling of these free carriers lowers the efficiency of radiative recombination and increases the probability of trapping at localized defects followed by nonradiative decay. Several reports suggest the existence of trap states, excitonic states, or free carrier states either between the E_2 and E_1 or in the gap.[34,36,39,40] For example, Ma et al. provide evidence for an electron–hole continuum between the first two excitonic states that is dipole-forbidden via single-photon excitation.[34] Such a mechanism is an intriguing possibility for protonated SWNTs, as a number of electric fields exist on the surface of such nanotubes. A proton localizes a small amount of electron density, producing a field normal to the SWNT's long axis at the site of protonation. Also, the heterogeneous distribution of protons along the SWNT axis will create a large number of local fields in the axial direction. The existence of such fields could serve to dissociate excitons, populating nonradiative states associated with an electron–hole continuum.[41] We reiterate that we suggest the above mechanisms as *intriguing possibilities* and that we do not have experimental data to confirm such mechanisms. Without further experimental evidence, one can conclude that a combination of the effects described above, as well as other mechanisms, may contribute to reducing the efficiency of the $E_2 \rightarrow E_1$ relaxation channel for protonated SWNTs. Clearly, further theoretical and experimental treatments are warranted.

Finally, to benchmark the performance of the bright, unprotonated raw SC-SWNTs relative to other literature reports, we compared the PL emission from several species to the luminescence from an IR26 reference dye solution. Single-species quantum yields were extracted by explicitly modeling the absorbance and PLE spectra as discussed previously.[7] A complete description of the methodology is given in the Supporting Information. The calculated quantum yields for several tube species are shown in Table 1. They range from ~0.9–1.4%, in accordance with recent reports on separated or selectively dispersed SWNTs.[12,13] We note that these quantum yields are calculated following subtraction of the large, nonresonant background in the absorbance spectrum and thus only depend on the resonant absorption into a particular (*n*,*m*) species. A recent study demonstrated a dramatic enhancement of the PL quantum yield for selectively dispersed SWNTs for which the nonresonant background was severely diminished.[13] Our data suggest that the SC surfactant is particularly well-suited for dispersing relatively bright SWNTs.

In conclusion, we have demonstrated that protonation affects the efficiency with which E_2 excitons relax to the luminescent E_1 state. The degree to which the $E_2 \rightarrow E_1$ branching ratio affects the SWNT PL quantum yield may be quite significant, especially in commonly used surfactants such as SDS or when there is residual protonation from, e.g., acid purification. Clearly, the $E_2 \rightarrow E_1$ efficiency cannot be assumed to be unity. By referencing to a standard infrared dye, IR26, we find φ_{PL} values as high as 1.4% for raw SWNTs dispersed in sodium cholate when absorption losses from the nonresonant background are considered. Solution-phase Raman spectroscopy is shown to be a powerful tool for determining the Fermi energy positions for samples with different purification and dispersion histories. The observations that the electronic properties of cholate-suspended SWNTs are not strongly perturbed suggests that this surfactant provides a micelle environment that is well isolated from the surrounding solvent. An improved understanding of this topic is crucial for understanding the inherent optical properties and processes intrinsic to the SWNTs and is critical for the utilization of SWNTs in important applications such as solar energy conversion.

Acknowledgment. This work was funded by the U.S. Department of Energy's Solar Photochemistry Program within the Office of Science, Office of Basic Energy Sciences, Division of Chemical Sciences, Geosciences, and Biosciences, under contract number DE-AC36-99GO10337 to NREL.

Supporting Information Available: Consideration of bundling for raw-SDS sample. Raman spectra of dry HiPCO powders. Effect of aging on SDS-dispersed SWNT samples. Calculation of SWNT quantum yield. This material is available free of charge via the Internet at http://pubs.acs.org.

References

(1) van de Lagemaat, J.; Barnes, T. M.; Rumbles, G.; Shaheen, S.; Coutts, T. J.; Weeks, C.; Levitsky, I.; Peltola, J.; Glatkowski, P. J. *Appl. Phys. Lett.* **2006**, *88*, 233503.
(2) Rowell, M. W.; Topinka, M. A.; McGehee, M. D.; Prall, H.-J.; Dennler, G.; Sariciftci, N. S.; Hu, L.; Gruner, G. *Appl. Phys. Lett.* **2006**, *88*, 233506.
(3) Aguirre, C. M.; Auvray, S.; Pigeon, S.; Izquierdo, R.; Desjardins, P.; Martel, R. *Appl. Phys. Lett.* **2006**, *88*, 183104/1.
(4) Misewich, J. A.; Martel, R.; Avouris, P.; Tsang, J. C.; Heinze, S.; Tersoff, J. *Science* **2003**, *300*, 783.
(5) Choi, J. H.; Nguyen, F. T.; Barone, P. W.; Heller, D. A.; Moll, A. E.; Patel, D.; Boppart, S. A.; Strano, M. S. *Nano Lett.* **2007**, *7*, 861.

(6) O'Connell, M. J.; Bachilo, S. M.; Huffman, C. B.; Moore, C. M.; Strano, M. S.; Haroz, E. H.; Rialon, K.; Boul, P. J.; Noon, W. H.; Kittrell, C.; Ma, J. P.; Hauge, R. H.; Weisman, R. B.; Smalley, R. E. *Science* **2002**, *297*, 593.
(7) Jones, M.; Engtrakul, C.; Metzger, W. K.; Ellingson, R. J.; Nozik, A. J.; Heben, M. J.; Rumbles, G. *Phys. Rev. B: Condens. Matter* **2005**, *71*, 115426.
(8) Wang, F.; Dukovic, G.; Brus, L. E.; Heinz, T. F. *Phys. Rev. Lett.* **2004**, *92*, 177401.
(9) Huang, L.; Pedrosa, H. N.; Krauss, T. D. *Phys. Rev. Lett.* **2004**, *93*, 017403.
(10) Heller, D. A.; Mayrhofer, R. M.; Baik, S.; Grinkova, Y. V.; Usrey, M. L.; Strano, M. S. *J. Am. Chem. Soc.* **2004**, *126*, 14567.
(11) Cognet, L.; Tsyboulski, D. A.; Rocha, J.-D. R.; Doyle, C. D.; Tour, J. M.; Weisman, R. B. *Science* **2007**, *316*, 1465.
(12) Crochet, J.; Clemens, M.; Hertel, T. *J. Am. Chem. Soc.* **2007**, *129*, 8058.
(13) Nish, A.; Hwang, J.-Y.; Doig, J.; Nicholas, R. J. *Nat. Nanotechnol.* **2007**, *2*, 640.
(14) Carlson, L. J.; Maccagnano, S. E.; Zheng, M.; Silcox, J.; Krauss, T. D. *Nano Lett.* **2007**, *7*, 3698.
(15) Lefebvre, J.; Austing, D. G.; Bond, J.; Finnie, P. *Nano Lett.* **2006**, *6*, 1603.
(16) Blackburn, J. L.; Engtrakul, C.; McDonald, T. J.; Dillon, A. C.; Heben, M. J. *J. Phys. Chem. B* **2006**, *110*, 25551.
(17) McDonald, T. J.; Jones, M.; Engtrakul, C.; Ellingson, R. J.; Rumbles, G.; Heben, M. J. *Rev. Sci. Instrum.* **2006**, *77*, 053104/1.
(18) Purchased from Exciton, Inc.
(19) Kopainsky, B.; Qiu, P.; Kaiser, W.; Sens, B.; Drexhage, K. H. *Appl. Phys. B: Lasers Opt.* **1982**, *29*, 15.
(20) Moore, V. C.; Strano, M. S.; Haroz, E. H.; Hauge, R. H.; Smalley, R. E. *Nano Lett.* **2003**, *3*, 1379.
(21) Strano, M. S.; Huffman, C. B.; Moore, C. M.; O'Connell, M. J.; Haroz, E. H.; Hubbard, J.; Miller, M.; Rialon, K.; Kittrell, C.; Ramesh, S.; Hauge, R. H.; Smalley, R. E. *J. Phys. Chem. B* **2003**, *107*, 6979.
(22) Zhuo, W.; Vavro, J.; Nemes, N. M.; Fischer, J. E.; Borondics, F.; Kamaras, K.; Tanner, D. B. *Phys. Rev. B: Condens. Matter* **2005**, *71*, 205423.
(23) Ramesh, S.; Ericson, L. M.; Davis, V. A.; Saini, R. K.; Kittrell, C.; Pasquali, M.; Billups, W. E.; Adams, W. W.; Hauge, R. H.; Smalley, R. E. *J. Phys. Chem. B* **2004**, *108*, 8794.
(24) McDonald, T. J.; Blackburn, J. L.; Metzger, W. K.; Rumbles, G.; Heben, M. J. *J. Phys. Chem. C* **2007**, *111*, 17894.
(25) Yan, J.; Zhang, Y.; Kim, P.; Pinczuk, A. *Phys. Rev. Lett.* **2007**, *98*, 166802.
(26) Abdula, D.; Nguyen, K. T.; Shim, M. *J. Phys. Chem. C* **2007**, *111*, 17755.
(27) Tsang, J. C.; Freitag, M.; Perebeinos, V.; Liu, J.; Avouris, P. *Nat. Nanotechnol.* **2007**, *2*, 725.
(28) Brown, S. D. M.; Jorio, A.; Corio, P.; Dresselhaus, M. S.; Dresselhaus, G.; Saito, R.; Kneipp, K. *Phys. Rev. B* **2001**, *63*, 155414.
(29) Jorio, A.; Filho, A. J. S.; Dresselhaus, G.; Dresselhaus, M. S.; Swan, A. K.; Unlu, M. S.; Goldberg, B. B.; Pimenta, M. A.; Hafner, J. H.; Lieber, C. M.; Saito, R. *Phys. Rev. B* **2002**, *65*, 155412.
(30) Yu, Z.; Brus, L. E. *J. Phys. Chem. A* **2000**, *104*, 10995.
(31) McDonald, T. J.; Engtrakul, C.; Jones, M.; Rumbles, G.; Heben, M. J. *J. Phys. Chem. B* **2006**, *110*, 25339.
(32) Engtrakul, C.; Davis, M. F.; Gennett, T.; Dillon, A. C.; Jones, K. M.; Heben, M. J. *J. Am. Chem. Soc.* **2005**, *127*, 17548.
(33) Weisman, R. B.; Bachilo, S. M. *Nano Lett.* **2003**, *3*, 1235.
(34) Ma, Y.-Z.; Valkunas, L.; Bachilo, S. M.; Fleming, G. R. *J. Phys. Chem. B* **2005**, *109*, 15671.
(35) Scholes, G. D.; Tretiak, S.; McDonald, T. J.; Metzger, W. K.; Engtrakul, C.; Rumbles, G.; Heben, M. J. *J. Phys. Chem. C* **2007**, *111*, 11139.
(36) Wang, F.; Dukovic, G.; Brus, L. E.; Heinz, T. F. *Science* **2005**, *308*, 838.
(37) Metzger, W. K.; McDonald, T. J.; Engtrakul, C.; Blackburn, J. L.; Scholes, G. D.; Rumbles, G.; Heben, M. J. *J. Phys. Chem. C* **2007**, *111*, 3601.
(38) Wang, F.; Dukovic, G.; Knoesel, E.; Brus, L. E.; Heinz, T. F. *Phys. Rev. B* **2004**, *70*, 241403.
(39) Satishkumar, B. C.; Goupalov, S. V.; Haroz, E. H.; Doorn, S. K. *Phys. Rev. B* **2006**, *74*, 155409.
(40) Lakoubovskii, K.; Minami, N.; Kim, Y.; Miyashita, K.; Kazaoui, S.; Nalini, B. *Appl. Phys. Lett.* **2006**, *89*, 173108.
(41) Mohite, A. D.; Gopinath, P.; Shah, H. M.; Alphenaar, B. W. *Nano Lett.* **2008**, *8*, 142.

NL072809G